Antibacterial and antiviral activities of SiO2-Ag and ZrO2-Ag nanocomposite coatings deposited on polymeric air filters

ARTICLE IN PRESS

Ceramics International xxx (xxxx) xxx

Contents lists available at ScienceDirect

Ceramics International

journal homepage: www.elsevier.com/locate/ceramint

Antibacterial and antiviral activities of SiO_2-Ag and ZrO_2-Ag nanocomposite coatings deposited on polymeric air filters

Domiziana Porporato [a,b,1], Angelica Luceri [c,1], Elisa Feyles [a], David Lembo [a], Manuela Donalisio [a,*], Borja Coto [d], Sofia Alves [d], Olatz Areitioaurtena [d], Per Persson [e], Cristina Balagna [c,**]

[a] Department of Clinical and Biological Sciences, Laboratory of Molecular Virology and Antiviral Research, University of Turin, Regione Gonzole 10, 10043, Orbassano, TO, Italy
[b] National PhD Program in One Health Approaches to Infectious Diseases and Life Science Research, Department of Public Health, Experimental and Forensic Medicine, University of Pavia, Pavia, 27100, Italy
[c] Applied Science and Technology Department, DISAT, Politecnico di Torino, Corso Duca degli Abruzzi 24, Turin, 10129, Italy
[d] Tekniker, Basque Research and Technology Alliance (BRTA), C/ Iñaki Goenaga 5, 20600, Eibar, Spain
[e] Department of Physics, Chemistry and Biology (IFM), Linköping University, Linköping, SE-581 83, Sweden

ARTICLE INFO

Keywords:
Antimicrobial
Antiviral
Composite coatings
Air filtration system

ABSTRACT

Acute respiratory infections are the most common cause of acute illness globally and have a severe impact on human health and productivity. There is robust evidence of airborne transmission of many respiratory viruses via direct or indirect contact with droplets and aerosol produced by infected individuals, and this transmission route becomes crucial in crowded indoor spaces. Heating, ventilating and air conditioning (HVAC) systems filters can reduce the concentration of virus-carrying droplets, but HVAC systems able to directly inactivate bacteria and viruses are highly desirable to preserve safe indoor air.

The aim of the present work was to assess the antibacterial and antiviral properties of silver nanoclusters/silica or zirconia composite coatings deposited onto polymeric air filters against *Staphylococcus epidermidis, Staphylococcus aureus* and a panel of representative members of human respiratory viruses, such as human coronavirus OC43 (HCoV-OC43), human rhinovirus A1 (HRV-A1), influenza virus type A (IFVA-H3N2) and adenovirus type −5 (AdV-5) according to standard protocols ISO.

Results evidenced that both coatings showed a significant antimicrobial and antiviral activity at variable extent and a good cytocompatibility on all the examined cell lines, demonstrating a broad-spectrum action against selected bacteria and respiratory viruses.

1. Introduction

Respiratory tract infections remain a leading cause of morbidity and mortality worldwide, particularly in densely populated indoor environments where airborne transmission is facilitated. Bioaerosols, airborne particles containing microorganisms such as bacteria, fungi, and viruses, pose a significant threat to public health, especially when ventilation is inadequate [1]. The most prevalent respiratory pathogens are human coronavirus OC43 (HCoV-OC43), human rhinovirus A1 (HRV-A1), influenza virus A (IFV-A H3N2), and adenovirus type 5 (AdV-5), which can cause a range of illnesses from mild colds to severe pneumonia. HCoV-OC43 primarily infects the upper respiratory tract, causing sore throat, cough and rhinorrhoea, and accounts for roughly the 15% of cases of common cold, but can evolve into more severe manifestations such as bronchitis and pneumonia, especially in children and elderly adults with underlying diseases [2]. HRV-A1 is the main

* Corresponding author.
** Corresponding author.
E-mail addresses: domiziana.porporato@unito.it (D. Porporato), angelica.luceri@polito.it (A. Luceri), elisa.feyles@unito.it (E. Feyles), david.lembo@unito.it (D. Lembo), manuela.donalisio@unito.it (M. Donalisio), borja.coto@tekniker.es (B. Coto), sofia.alves@tekniker.es (S. Alves), olatz.areitioaurtena@tekniker.es (O. Areitioaurtena), per.persson@liu.se (P. Persson), cristina.balagna@polito.it (C. Balagna).
[1] These authors contributed equally to this work.

https://doi.org/10.1016/j.ceramint.2026.04.139
Received 26 November 2025; Received in revised form 8 April 2026; Accepted 10 April 2026
Available online 12 April 2026

etiologic agent of common cold (causing from 30% to 50% of all cases) [3], however, in the last two decades, HRV has been reported as one of the main viral causes for severe lower respiratory tract respiratory illnesses that may require hospitalization. Moreover, HRV can be associated with exacerbations of chronic respiratory illnesses such as asthma and chronic obstructive pulmonary disease (COPD) [4]. IFV-A alone causes 3 to 5 million severe cases and 290000 to 650000 deaths every year due to respiratory disease [5]. In particular, IFV-A H3N2 occurred for the first time in 1968 and has continually circulated in the human population, currently being the major cause of seasonal influenza morbidity and mortality [6]. AdV-5 is a common cause of respiratory illness and pneumonia in children and can also be responsible for nosocomial outbreaks in paediatric respiratory units, with a mortality rate among such children, who often have coexistent respiratory disease, ranging from 20% to 39% [7].

The majority of exhaled aerosols is smaller than 5 μm and may contain infectious viruses that are transported in the air according to environmental factors as temperature, humidity, airflow and ventilation, and cause several infectious diseases reaching the respiratory tract [8]. In fact, there is robust evidence of airborne transmission of many respiratory viruses through droplets and aerosols, which can be generated by infected individuals during various activities such as breathing, talking and coughing [9,10].

While conventional air filtration systems such as HEPA and HVAC filters can physically trap airborne pathogens, they lack intrinsic antimicrobial properties [11]. This limitation allows microorganisms to survive and potentially proliferate on filter surfaces, posing a risk of secondary contamination [12,13]. Consequently, recent advances in antimicrobial and antiviral filtration have shifted the focus toward active neutralization through sophisticated nanostructures and photobiocidal mechanisms. A significant breakthrough in this field involves the use of dual-action nanoblades integrated into PPE masks, which, as demonstrated by Park et al. [14], can rapidly inactivate airborne pathogens via combined mechanical puncturing and localized photothermal heating, obtaining achieved >99% kill of *S. epidermidis*. In parallel, light-driven strategies have shown great promise; for instance, the generation of reactive oxygen species (ROS) via visible light has been successfully harnessed through both transparent electrospun nanofibers embedded with crystal violet [15] and TiO_2/reduced graphene oxide (rGO) composites [16]. These latter materials are particularly effective as the rGO additive enables ROS production even from the minimal UV component of white light, leading to significant log reductions in both bacterial and viral loads.

The integration of multifunctionality is also a key trend, with recent developments in silica–alumina coatings that combine photosensitizers with triboelectric charging to enhance particle capture and maintain high inactivation rates even after washing [17]. They showed more than 99% inactivation of both *S. epidermidis* and *E. coli* bacteria, and MS2 bacteriophage under illumination.

The current frontier of research emphasizes the synergy between biocide activity and surface morphology. For instance, the development of petal-like nanostructures (PNSs) has enabled the creation of multifunctional fabrics that combine visible-light-activated antimicrobial properties with superhydrophobic-based antifouling activities [18].

Despite the potential of these emerging light-driven and structural strategies, silver (Ag) remains a cornerstone in antimicrobial research due to its unparalleled broad-spectrum efficacy and long-standing reliability. However, the challenge has evolved from simply using silver to optimizing its integration into filter media to ensure stability and sustained activity. To address this, recent efforts have focused on incorporating silver nanoparticles (AgNPs) directly into filter materials to achieve a dual functionality of physical filtration and active pathogen inactivation [19]. Various forms of silver, from thin coating to nanoparticles, have been widely used as antimicrobial and antiviral agents, for their strong efficacy [20–23]. Park et al. [24] developed an AgNPs-doped coating for air filters used in subway filtration systems. The filters resulted effective against aerosolized MS2 bacteriophage particles and its filtration performance was not affected by the presence of the nanoparticles. In addition, a method based on recoating the antiviral material through an aerosol process, was proposed, for regenerating the antiviral activity of the filters, resulting simply applicable [24]. The use of composite systems, embedding silver nanoparticles into a matrix, let to avoid dispersion and agglomeration of them, thus improving chemical stability and mechanical behavior. Several studies have shown that AgNPs-doped silica systems exhibit strong antibacterial activity, in some cases even superior to the use of AgNPs alone, mainly due to the controlled and prolonged release of Ag^+ ions from the silica matrix. In addition, when applied in air filtration systems, Ag–silica nanocomposites provided effective antimicrobial and antiviral properties, with efficiencies above 90%, without significantly compromising the overall filtration performance [25].

Moreover, great attention is given to the production methods of these systems, with a strong focus on eco-friendly and sustainable methods, aiming to minimize environmental impact and the use of hazardous chemicals [26,27]. Among the green processes, the magnetron sputtering technique allows the production of very thin films suitable for various materials, imparting specific properties, including antibacterial and antiviral ones [28–30]. AgCu nanometric films have been deposited onto thin polypropylene filters via magnetron sputtering, demonstrating strong antiviral efficacy against the SARS-CoV-2 virus and antibacterial activity against pathogens, without being cytotoxic to humans [31]. The coating has been tested against bioaerosols loaded with aerobic and anaerobic bacteria, oral pathogens, and surrogate models of respiratory viruses, and showed a high inhibition rate within 8 h for SARS-CoV-2 (95.6%) and near-complete inactivation of the surrogate virus (almost 100%), and excellent antimicrobial properties against pathogenic bacteria, making coating effective in improving the protective capabilities of devices, such as protective equipment [31]. The high-vacuum roll-to-roll magnetron sputtering technique has also been used to coat non-woven fabrics for face masks with ultra-thin Ag and Cu films [32], showing high efficiency in inhibiting and inactivating *E. coli* and *S. aureus*, and influenza A H1N1 virus. Furthermore, by studying the color change of the masks worn by patients with rhinitis for 2 h, caused by NOx in the breath that oxidize the Ag in the masks, the coating shows potential in monitoring the conditions of respiratory diseases.

In this context, the present study aims to systematically evaluate the antiviral and antibacterial performance of polymeric air filters coated with silver nanoclusters embedded in silica (SiO_2) or zirconia (ZrO_2) matrices. SiO_2 and ZrO_2 were selected as oxide matrices because of their chemical stability and their capability to stabilize Ag nanoclusters within nanocomposite coatings, while providing different structural environments that may influence antimicrobial performance. Moreover, both oxides can be efficiently deposited by magnetron sputtering on polymeric substrates such as polyethylene terephthalate (PET), which is widely used in air filtration media. This makes them particularly suitable for the fabrication of antimicrobial coatings directly on filter materials.

While Ag-based nanocomposite coatings have been previously investigated [33–36], comprehensive studies assessing their antiviral activity against multiple respiratory viruses under standardized ISO protocols remain limited. In this work, the coatings were therefore tested against a panel of representative respiratory viruses belonging to different viral families, including both enveloped and non-enveloped viruses (HCoV-OC43, HRV-A1, IFVA-H3N2 and AdV-5) and bacteria (*S. epidermidis*, *S. aureus*), in order to provide a robust and standardized validation of their broad-spectrum antiviral potential for air filtration applications.

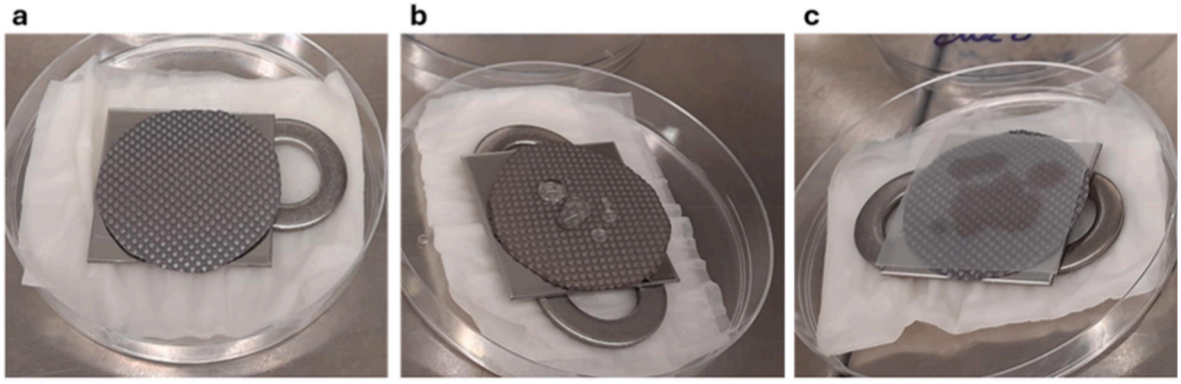

Fig. 1. Illustration of the methodology used to evaluate the viability of *S. aureus* in contact with the reference and treated filters following ISO 20743 and 22196 guidelines (a) PET-treated testing filter facing upwards on aluminium sheet placed on stainless-steel cylinders to provide stability and over wet Kimberly Clark precision wipes to avoid dryness, (b) *S. aureus* inoculum on testing filter, (c) parafilm placed over the inoculum to guarantee surface contact.

2. Materials and Methods

2.1. Coating deposition

Silica or zirconia composite coatings containing silver nanoclusters were deposited on polyethylene terephthalate air filter (PET, supplied by GV Filtri) through radio-frequency co-sputtering equipment (Kenosistec™). Two targets operated simultaneously, one used for the matrix deposition, in silica, SiO_2 (99.99% SiO_2, Nanovision™) or zirconia ZrO_2, (99.98% ZrO_2, Nanovision™), and the second one for silver deposition (9.99% Ag, 5 Pa™). The process, conducted following a patented procedure [37], lasted 1 h in a controlled argon (Ar) atmosphere. Specifically, RF power of 200 W and 250 W was applied for silica and zirconia matrices, respectively, while 4 W of DC power was applied to the silver target.

2.2. Compositional and morphological analysis

The elemental composition of the obtained coatings was verified using Energy Dispersive X-ray Spectrometry (EDS), which quantified the atomic percentage (at.%) of Ag, as well as Si and Zr, the elements constituting the oxide matrix. For each coating, three areas were evaluated at a magnification of 150× to ensure statistical reliability.

The morphological aspect of the coatings and the uncoated filter was analyzed using a Field Emission Scanning Electron Microscope (FESEM, Quanta Inspect 200, Zeiss Supra 40™). Analysis at different magnifications allowed for the assessment of potential differences between the two studied matrices and the dispersion of silver nanoclusters within them. Scanning Transmission Electron Microscopy (STEM) analysis was conducted on both coatings, which were deposited onto TEM-specific support, using a FEI HeliosNanoLab dual-beam focused ion beam (FIB) microscope. The microstructure and elemental distribution of the samples were examined at the atomic level through high-angle annular dark-field (HAADF) STEM imaging, energy-dispersive X-ray spectroscopy (EDX) and electron energy-loss spectroscopy (EELS) mapping. These investigations were conducted using the Linköping FEI Titan3 60-300 microscope, operating at 300 kV, and fitted with a Super-X EDX system and a Gatan GIF Quantum ERS post-column imaging filter, and allowed the evaluation of the size of the silver nanoclusters and their distribution within the matrix.

2.3. Antibacterial analysis

2.3.1. Inhibition halo test

The antibacterial effect of the coated filter was evaluated using the inhibition halo test, a qualitative and rapid assay performed according to the NCCLS M2-A9 standard [38]. The test was conducted against the non-pathogenic Gram-positive bacterium *Staphylococcus epidermidis* (ATCC 14990).

A standardized bacterial solution containing 1×10^8 CFU/mL, corresponding to 0.5 on the McFarland scale, assessed by an optical photometer (Phoenix Spec BD McFarland was evenly spread onto the surface of a nutrient agar plate, and both uncoated and coated membrane samples (1×1 cm^2) were placed in direct contact with the agar, ensuring that the coated surface faced the bacterial solution.

Bacterial growth or inhibition was assessed after 24 h of incubation at 35 °C, analyzing the presence and the size of the halo.

2.3.2. Bacterial viability test

The antibacterial activity of the coated filters was also evaluated using a quantitative test based on ISO 20743 [39] guidelines for textile materials. Given the high absorption capacity of the PET filter material, the absorption method was utilized. This approach was critical to ensure proper sample incubation while preventing dryness, which was managed using Kimberly Clark precision wipes. Bacterial recovery from both uncoated and coated filters followed standard procedures, utilizing 10 mL of Soybean-Casein Digest Lecithin Polysorbate broth (SCDLP) solution and sterile bags to prevent bacterial retention within the filter. The procedure also incorporated aspects of ISO 22196 [40], a standard recognized for antimicrobial surface coatings, to maximize bacterial recovery. In summary, a bacterial suspension of Gram-positive bacteria *Staphylococcus aureus* (ATCC 6538) was prepared and inoculated (0.2 mL) onto the filter surface (1134 mm^2) at approximately 1-3 $\times$ 10^5 CFU/mL. A cover film was applied on the top of the inoculum to distribute it evenly, and the sample was incubated for 20 h at 35 °C ± 2 °C with 95% relative humidity. These steps are outlined in Fig. 1.

After incubation, the cover film was removed, and the samples were washed in 10 mL of SCDLP solution for bacterial recovery. The suspension was then plated onto agar PCA plates and incubated for 20 h at 35 °C ± 2 °C. Colony growth was assessed to determine the bacterial load on the surfaces. The number of viable bacteria on the uncoated and coated filters was used to calculate antibacterial activity in terms of the R value and inhibition percentage. The R value represents bacterial reduction by comparing the number of bacteria recovered from untreated filters to those recovered from treated filters on a logarithmic scale, and, if the test has a positive effect, this value is calculated according to the following formula:

$$R = [\log(A / B) - \log(C / A)] = [log(B / C)] \quad (1)$$

Equation (1). Calculation of antibacterial activity (R value) based on the logarithmic reduction of viable bacteria on treated versus untreated samples.

Where.

Table 1
Atomic percentage of Si, Zr and Ag of the uncoated and silver/silica or zirconia coated PET air filter.

Sample	Si (% at.)	Zr (% at.)	Ag (% at.)
UC	/	/	/
SiO_2-Ag	4.3 ± 0.1	/	3.6 ± 0.5
ZrO_2-Ag	/	1.5 ± 0.1	1.5 ± 0.1

- *A = average of the number of viable bacteria cells counted immediately after inoculation on the untreated test piece;*
- *B = average of the number of viable bacteria cells on the untreated test piece after 20 ± 2 h;*
- *C = average of the number of viable bacteria cells on the antimicrobial test piece after 20 ± 2 h.*

Before testing, both sides of the filters and cover films were sterilized by UV radiation in a laminar airflow chamber for 10 min.

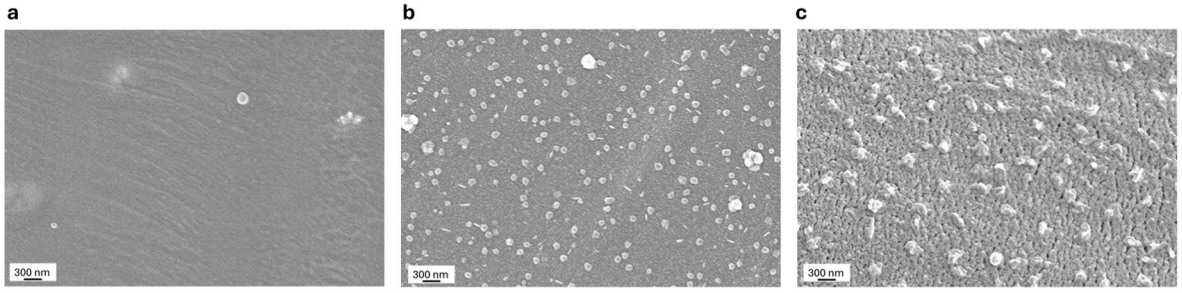

Fig. 2. FESEM images of (**a**) uncoated PET filter, (b) PET filter with SiO_2-Ag coating and (c) ZrO_2-Ag coating.

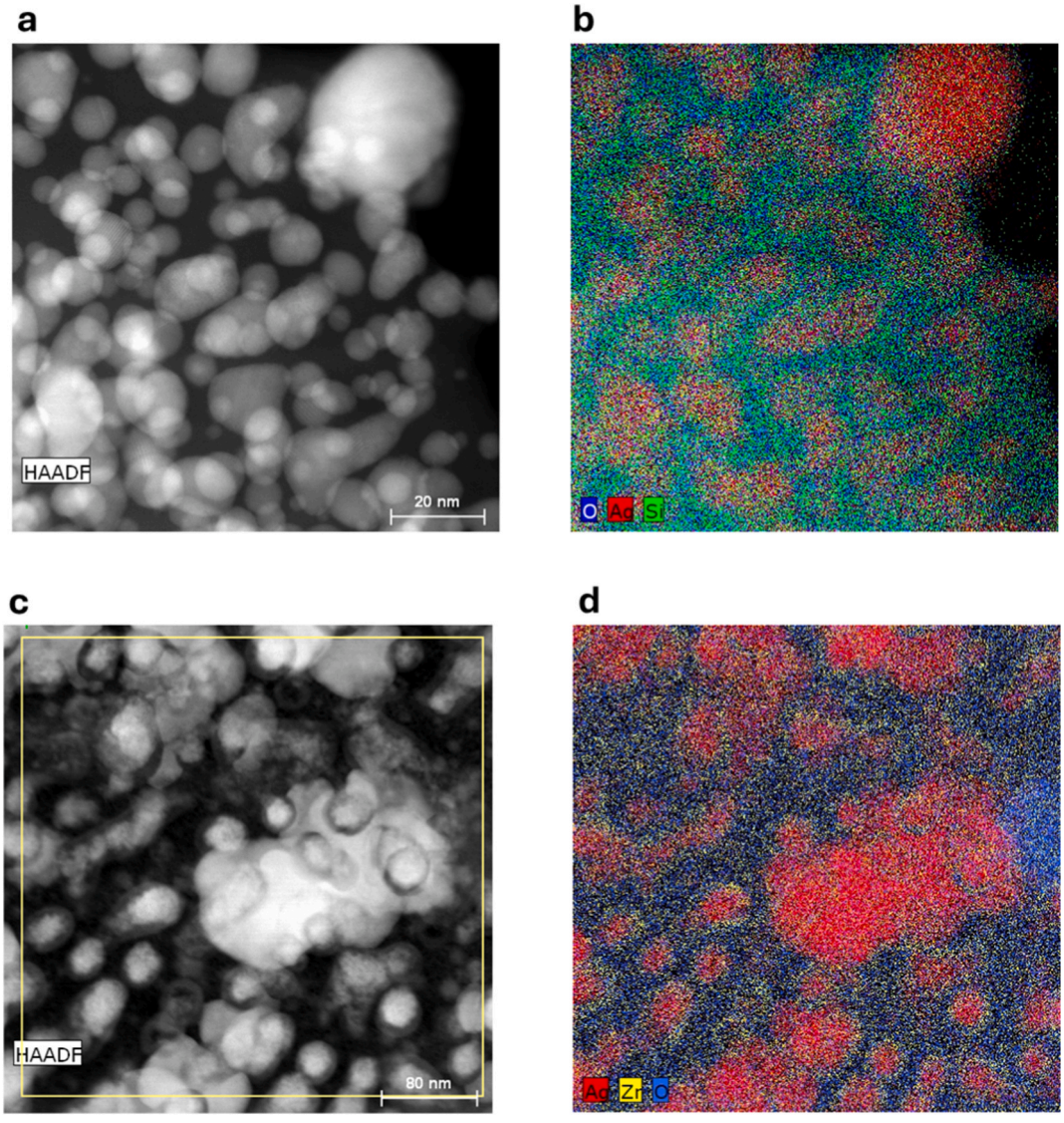

Fig. 3. HAADF-STEM micrograph of (a) SiO_2-Ag coating and (c) ZrO_2-Ag coating and (b, d) corresponding EDX maps.

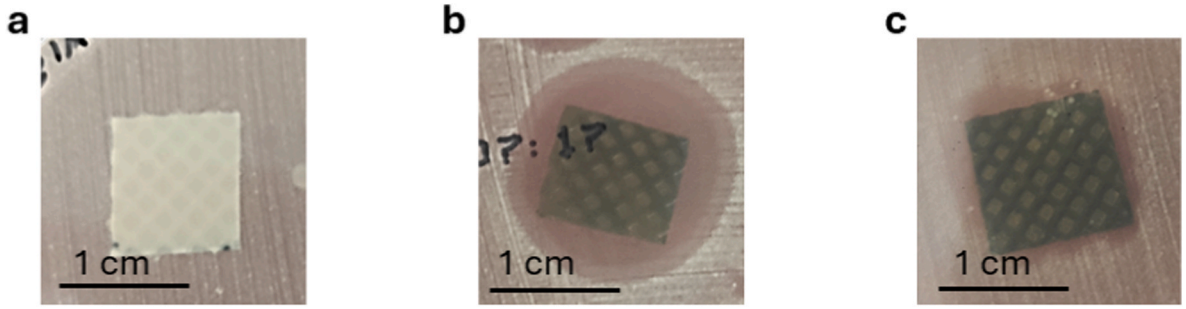

Fig. 4. Inhibition halo test against *S. epidermidis* of (**a**) uncoated PET filter, (b) SiO_2-Ag coating and (c) ZrO_2-Ag coating.

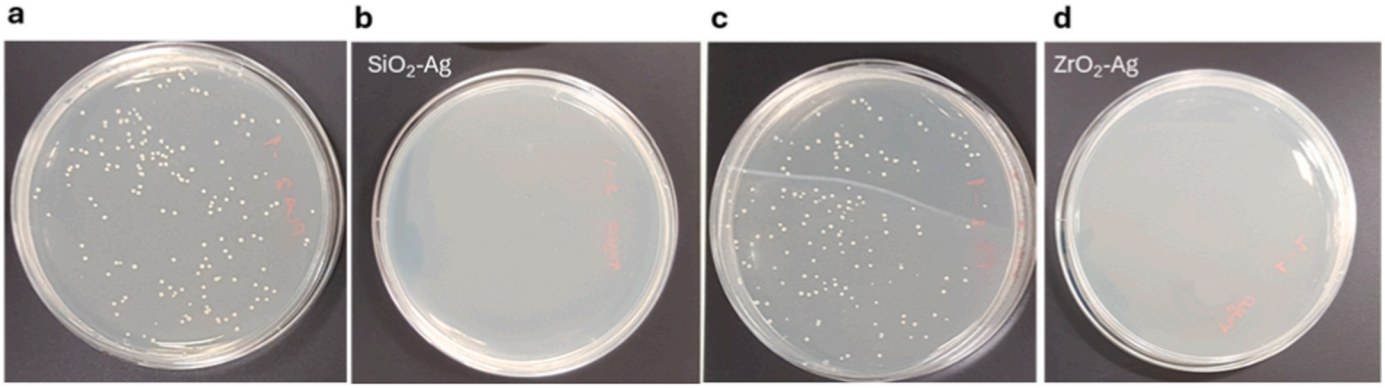

Fig. 5. Antibacterial test representative results of (a) PET filter control for SiO2-Ag testing, (b) SiO_2-Ag coated filter, (c) PET filter control for ZrO_2-Ag testing and (d) ZrO_2-Ag coated filters.

Table 2
Results of the antibacterial activity of SiO_2-Ag and ZrO_2-Ag coatings against *S. aureus* bacteria expressed in R value and inhibition %.

Sample	CFU/cm2 20h incubation	R value	Inhibition %
UC	1.49×10^4	3.19	99.94
SiO_2-Ag	9.58×10^0		
UC	1.26×10^4	3.15	99.93
ZrO_2-Ag	8.82×10^0		

UC: uncoated.

2.4. Antiviral properties evaluation

2.4.1. Cell lines and viruses

Human lung fibroblasts (MRC-5) (ATCC® CCL-171™) were utilized for the production of human beta-coronavirus, type OC43 (HCoV-OC43, ATCC® VR-1558™). Human cervix adenocarcinoma cells (HeLa) (ATCC® CCL-2™) were used for the cultivation of human rhinovirus, type A1 (HRV-A1, ATCC® VR-1559™) and adenovirus, type 5 (AdV-5, ATCC® VR-5™). Madine-Darby canine kidney epithelial cells (MDCK) (ATCC® CCL-34™) were used for the production of Influenza virus, type A (IFVA-H3N2, A/ChristChurch/28/03, Italian National Institute of Health). Cells were cultured in Dulbecco's Modified Eagle Medium (DMEM; Sigma Aldrich) supplemented with heat-inactivated, 10% (v/v) fetal bovine serum (FBS; Sigma Aldrich) in a humidified 5% CO_2 incubator. Culture medium was supplemented with 1% (v/v) antibiotic-antimycotic solution (Zell Shield, Minerva Biolabs, Berlin, Germany).

2.4.2. Virus production

HCoV-OC43, HRV-A1, and AdV-5 were produced using DMEM, supplemented with heat-inactivated, 2% (v/v) FBS, in a humidified 5% CO_2 incubator. IFVA-H3N2 was produced using DMEM, supplemented with 1 μg/mL of trypsin (Sigma Aldrich), in a humidified 5% CO_2 incubator. Briefly, cells were seeded in tissue culture flasks at the optimal 80% sub-confluency. The following day, HCoV-OC43, HRV-A1, AdV-5, IFVA-H3N2 were inoculated at multiplicity of infection (MOI) 0.1 on the appropriate cell line, and flasks were incubated at 34 °C (HCoV-OC43, HRV-A1) or 37 °C (IFVA-H3N2, AdV-5). When complete cytopathic effect (CPE) occurred, supernatants and cells were harvested, pooled, frozen-thawed three times, then clarified and aliquoted. IFVA-H3N2 and AdV-5 were concentrated by centrifugation (19,000g for 3h) before being aliquoted. Viral stocks were stored at −80 °C.

2.4.3. Virus titration

Viral titers were determined by standard focus assay (HCoV-OC43, HRV-A1, IFVA-H3N2) or standard plaque assay (AdV-5). Briefly, cells were seeded in 96-well plates, and then infected with serially diluted virus suspensions. For AdV-5, virus inoculum was removed after 2h at 37 °C, and monolayers of cells were overlaid with SeaPlaque® Agarose (Lonza) and incubated for 96h at 37 °C. AdV-5 plaques were visualised by fixing with formaldehyde 7.5% and staining with 0.1% of crystal violet in 20% ethanol. For HCoV-OC43, HRV-A1 and IFVA-H3N2, virus inoculum was removed after 16h at 34 °C, 24h at 34 °C or 16h at 37 °C, respectively. Single infected cells were detected by indirect immuno-peroxidase staining procedure as reported in *Baroni* et al. [41]. Specific primary antibodies were incubated for 1h at room temperature. The primary antibody for HRV-A1 was purchased from QED Bioscience (18758; SanDiego, CA), the primary antibody for HCoV-OC43 was purchased from Merck (MAB9013; Darmstadt, Germany), the primary antibody for IFVA-H3N2 was purchased from Abcam (ab20343; Boston, MA). The secondary antibody was incubated for 1h 20min at 37°. For all the viruses the secondary antibody peroxidase-conjugated AffiniPure F (ab')2 Fragment goat anti-mouse IgG (H + L) was purchased from Jackson ImmunoResearch Laboratories Inc. (West Grove, PA). Infected cells or viral plaques were microscopically counted, and viral titers were expressed as focus-forming unit (FFU) per mL (HCoV-OC43, HRV-A1,

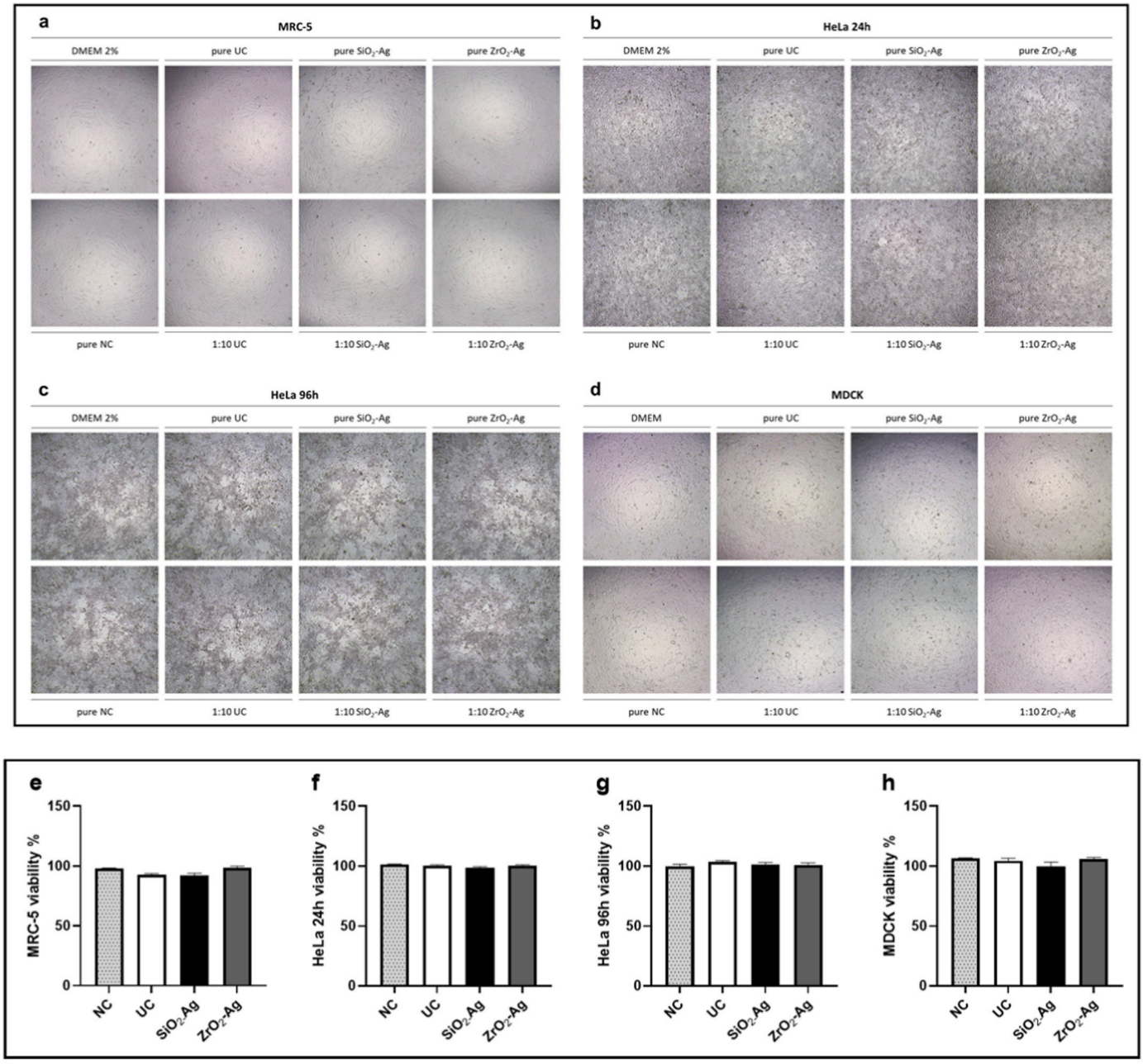

Fig. 6. SiO_2-Ag and ZrO_2-Ag coatings showed a good cytocompatibility profile on different cell lines. Cytotoxicity assessment was performed on MRC-5 for (**a**, **e**) HCoV-OC43, (**b**, **f**) HeLa 24h for HRV-A1,(**c**, **g**) HeLa 96h for AdV-5 and (**d**, **h**) MDCK for IFV-A H3N2. (**a-d**) Cytotoxic effect of coated filters on host cells was qualitatively analyzed under microscope observation as reported in ISO guideline. Magnification, 400×. DMEM, culture medium; DMEM 2%, culture medium supplemented with 2% of serum; pure, pure wash-out solution; 1:10, 1:10 diluted wash-out solution. **(e–h)** Cellular viability was quantified by MTS assay. Viability is reported on Y-axis and expressed as a percentage (cell viability %). Sample type is reported on X-axis. NC, negative control; UC, uncoated. The obtained results are the mean of two biological replicates. Additional details of the assays protocol are reported in the Materials and Methods section.

IFVA-H3N2) or plaque-forming unit (PFU) per mL (AdV-5).

2.4.4. Control test for the verification of cytotoxic effect of coatings on host cells

To determine the potential cytotoxic effect of the two coatings on host cells experiments were performed according to the ISO 21702:2019 (E) [42]. In detail, four washes with 10 mL of soybean casein digest broth with lecithin and polyoxyethylene sorbitan monooleate (SCDLP broth) diluted 1:200 in DMEM 2% FBS (or DMEM in case of MDCK) were performed on materials with SiO_2-Ag or ZrO_2-Ag coatings and on the uncoated material. 10 mL of diluted broth that did not contact any material were used as negative control. Cells were seeded in 96-well plates and treated with pure or 1:10 diluted wash-out solutions for 1h at 34 °C (MRC-5, HeLa for HRV-A1), 1h at 37 °C (MDCK) or 2h at 37 °C (HeLa for AdV-5). After a wash with culture medium, DMEM 2% FBS (MRC-5, HeLa for HRV-A1), DMEM (MDCK), or Sea Plaque (HeLa for AdV-5) was added to cells, which were then incubated for 16h or 24h at 34 °C (MRC-5, HeLa for HRV-A1),16h or 96h at 37 °C (MDCK, HeLa for AdV-5). Cell viability was observed with an optical microscope in order to evaluate alterations of treated cell monolayers.

2.4.5. Cell viability assay

Cell viability was measured using the MTS [3-(4,5-dimethylthiazol-2-yl)-5-(3-carboxymethoxyphenyl)-2-(4-sulfophenyl)-2H-tetrazolium]

Table 3
Numerical results of the second control test required by the ISO 21702:2019(E) guidelines.

Virus	Sample	Titer (FFU/mL or PFU/mL)	Log (Titer)
HCoV-OC43	**NC**	3.03×10^5	5.48
	UC	3.41×10^5	5.53
	SiO_2-Ag	2.08×10^5	5.32
	ZrO_2-Ag	2.09×10^5	5.32
HRV-A1	**NC**	6.44×10^5	5.81
	UC	5.49×10^5	5.74
	SiO_2-Ag	6.58×10^5	5.82
	ZrO_2-Ag	6.01×10^5	5.78
AdV-5	**NC**	3.00×10^6	6.48
	UC	3.37×10^6	6.53
	SiO_2-Ag	2.61×10^6	6.42
	ZrO_2-Ag	2.07×10^6	6.32
IFV-A H3N2	**NC**	3.45×10^4	4.54
	UC	2.87×10^4	4.46
	SiO_2-Ag	2.39×10^4	4.38
	ZrO_2-Ag	1.91×10^4	4.28

NC: negative control; UC: uncoated.

assay. Four washes with 10 mL of SCDLP broth diluted 1:200 in DMEM 2% FBS (or DMEM in case of MDCK) were performed on materials with SiO_2-Ag or ZrO_2-Ag coatings and on the uncoated material, 10 mL of diluted broth that did not contact any material were used as negative control. Cells were seeded in 96-well plates and incubated with pure or 1:10 diluted wash-out solutions, under the same experimental conditions used for the control test for the verification of cytotoxic effect of coatings on host cells. Cell viability was determined as reported in Francese et al. [43]. The effect on cell viability at different concentrations of the compound was expressed as a percentage, by comparing absorbances of cells incubated with the wash-out solutions with those of cells incubated with culture medium alone.

2.4.6. Control test for the verification of cell sensitivity to virus and the inactivation of antiviral activity by SCDLP broth

To verify the cell sensitivity to the virus and the inactivation of antiviral activity, experiments were performed according to the ISO 21702:2019(E). Four washes with 10 mL SCDLP broth diluted 1:200 in DMEM 2% FBS (or DMEM in case of IFVA-H3N2) were performed on the materials with SiO_2-Ag or ZrO_2-Ag coatings and on the uncoated material. 10 mL of diluted broth that did not contact any material was used as a negative control. 50 µL of pure virus was added to 5 mL of each wash-out solution. Test and control conditions were incubated for 30' at 25 °C. Next, virus suspensions were titrated, and viral titers were calculated as previously described. The viral titers were calculated by the mean of 8 technical replicates.

2.4.7. Antiviral assays

The protocol of antiviral assays complies with what is reported in the ISO 21702:2019(E) [37]. In detail, 400 µL of the viral stock (titer of 10^8 FFU or PFU/mL) were deposited on a 5 × 5cm square of material with the coating or on the uncoated material. The viral suspension was covered by a stomacher bag (cut in a square of 4 × 4cm), creating a thin film to maximize the contact with the material and to avoid virus evaporation. Four washes with 10 mL of SCDLP broth diluted 1:200 in DMEM 2% FBS (or DMEM in case of IFVA-H3N2) were performed to collect the virus at different time-points: immediately (only for the uncoated material) or after 24h at 25 °C (for coated and uncoated material) in a humidified 5% CO2 incubator (humidity >90%). Next, virus suspensions were titrated, and viral titers were calculated as previously described.

The viral titer on cm^2 of surface (FFU/cm^2 or PFU/cm^2) was calculated using the following formula:

$$T_{surface} = [T_{susp} * V] / A \quad (2)$$

Equation (2). Calculation of viral titer per surface area (T_surface) based on the viral concentration in the wash-out solution, the elution volume, and the sample surface area.

Where.

- $T_{surface}$ = *viral titer recovered* per *cm^2 of material [FFU cm^{-2} or PFU cm^{-2}];*
- T_{susp} = *viral titer recovered* per *mL of wash-out solution[FFU mL^{-1} or PFU mL^{-1}];*
- *V = volume of diluted SCDLP broth added to the specimen [mL];*
- *A is the surface area of the cover film [cm^2].*

The viral titers were calculated by the mean of 8 technical replicates.

Antiviral activity was expressed as R value:

$$R = [log_{10}\ T_{coated,24h} - log_{10}\ T_{uncoated,0h}] - [log_{10}\ T_{uncoated,24h} - log_{10}\ T_{uncoated,0h}] \quad (3)$$

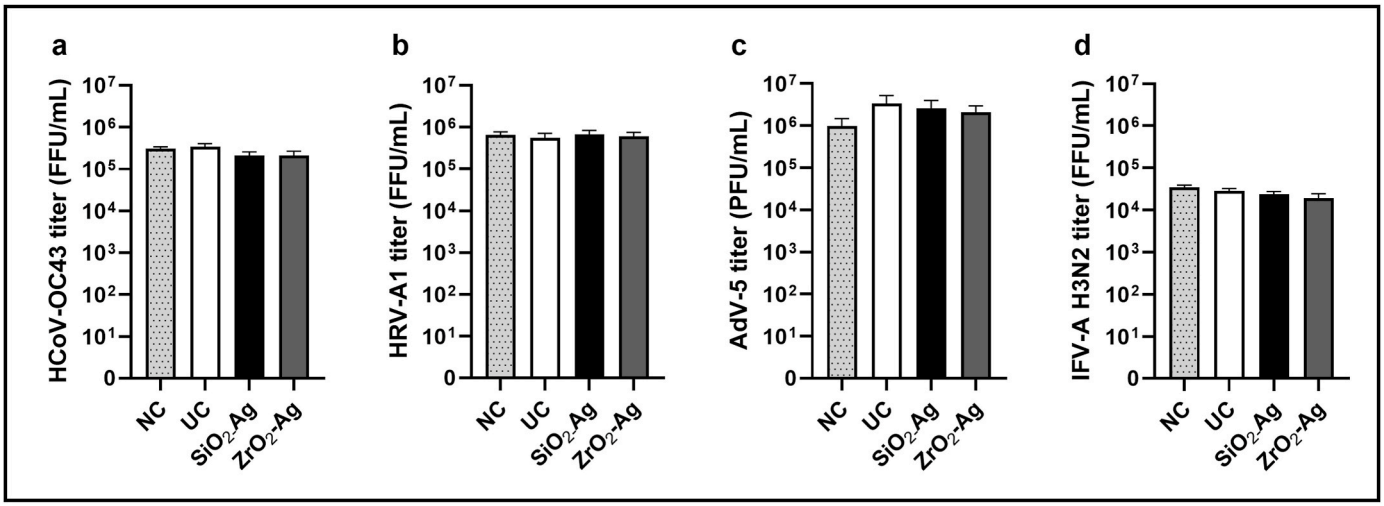

Fig. 7. SCDLP broth inactivated the potential antiviral activity of the coated materials, and cell sensitivity to virus infection was not modified. Control tests were conducted against (a) HCoV-OC43, (b) HRV-A1, (c) AdV-5, (d) IFV-A H3N2. Viral titer retrieved by wash-out solutions after 30 min at 25 °C of incubation is reported on the Y-axis and expressed as focus-forming unit or plaque-forming unit per mL (FFU or PFU/mL). Sample type is reported on the X-axis. NC, negative control; UC, uncoated. The obtained results are the mean of two biological replicates. Additional details of the assay protocol are reported in the Materials and Methods section.

Table 4
Numerical results of antiviral assays conducted following the ISO 21702:2019 (E) guidelines.

Virus	Sample	Titer (FFU/mL or PFU/mL)	Titer (FFU/cm^2 or PFU/cm^2)	R value	Inhibition %
HCoV-OC43	**UC Imm.**	4.51×10^6	2.82×10^6	-	-
	UC	3.37×10^5	2.11×10^5	-	-
	SiO_2-Ag	8.13×10^0	5.08×10^0	4.26	99.99
	ZrO_2-Ag	1.88×10^0	1.17×10^0	5.26	99.99
HRV-A1	**UC Imm.**	1.52×10^6	9.49×10^5	-	-
	UC	5.63×10^5	3.52×10^5	-	-
	SiO_2-Ag	8.74×10^2	5.46×10^2	2.81	99.84
	ZrO_2-Ag	9.22×10^2	5.76×10^2	2.79	99.84
AdV-5	**UC Imm.**	4.21×10^6	2.63×10^6	-	-
	UC	4.32×10^6	2.70×10^6	-	-
	SiO_2-Ag	4.97×10^5	3.11×10^5	0.94	88.48
	ZrO_2-Ag	7.05×10^5	4.40×10^5	0.79	83.68
IFV-A H3N2	**UC Imm.**	1.45×10^5	9.07×10^4	-	-
	UC	1.80×10^3	1.17×10^3	-	-
	SiO_2-Ag	2.50×10^0	1.56×10^0	2.88	99.87
	ZrO_2-Ag	1.13×10^1	7.04×10^0	2.22	99.40

UC Imm.: uncoated immediately collected; UC: uncoated.

Table 5
Summary of the antiviral activity of SiO_2-Ag and ZrO_2-Ag coatings against respiratory viruses expressed in R value and inhibition %.

Coating	Virus	R value	Inhibition %
SiO_2-Ag	*HCoV-OC43*	4.26	99.99
	HRV-A1	2.81	99.84
	AdV-5	0.94	88.48
	IFV-A H3N2	2.88	99.87
ZrO_2-Ag	*HCoV-OC43*	5.26	99.99
	HRV-A1	2.79	99.84
	AdV-5	0.79	83.68
	IFV-A H3N2	2.22	99.40

Equation (3). Calculation of antiviral activity (R value) and inhibition percentage based on the logarithmic reduction of viral titers on coated versus uncoated materials.

Where.

- $T_{coated,\ 24h}$ = *viral titer collected from coated material after 24 h at 25 °C [FFU cm^{-2} or PFU cm^{-2}];*
- $T_{uncoated,\ 0h}$ = *viral titer immediately collected from uncoated material (time 0) [FFU cm^{-2} or PFU cm^{-2}];*
- $T_{uncoated,\ 24h}$ = *viral titer collected from uncoated material after 24 h at 25 °C [FFU cm^{-2} or PFU cm^{-2}];*

and inhibition percentage

$$Inhibition\ (\%) = 100 - \left(T_{coated,24h} \ / \ T_{uncoated,24h} \times 100\right) \quad (4)$$

Equation (4). Calculation of viral inhibition percentage based on the ratio of viral titers on coated and uncoated materials after 24 h of contact.

Where.

- $T_{coated,\ 24h}$ = *viral titer collected from coated material after 24 h at 25 °C [FFU cm^{-2} or PFU cm^{-2}];*
- $T_{uncoated,\ 24h}$ = *viral titer collected from uncoated material after 24 h at 25 °C [FFU cm^{-2} or PFU cm^{-2}];*

2.4.8. Statistical analyses

Statistical analyses were performed using GraphPad PRISM 10.2.2 (GraphPad Software, San Diego, CA, USA). Ordinary one-way ANOVA test was used to assess the statistical significance of the differences between the viral titers of virus incubated with coated and uncoated materials. Significance was set at the 95 % level.

3. Results and discussion

3.1. Compositional and morphological analysis

The sputtering deposition process was successfully carried out for both silica-based and zirconia-based coatings on PET air filters. The results of the compositional analysis by EDS are shown in Table 1.

For the uncoated filter, which was primarily composed of carbon (C) and oxygen (O), no traces of silicon (Si), zirconium (Zr), or silver (Ag) were detected. In contrast, the silicon content in the silver/silica coatings was 4.3 ± 0.1 at.%, while the zirconium content in the silver/zirconia coatings was around 1.5 ± 0.1 at.%. Silver content was 3.6 ± 0.5 at.% in the silica coatings and 1.5 ± 0.1 at.% in the zirconia coatings. Fig. 2 shows the morphology of the air filters before and after the coating deposition. The uncoated sample exhibits a smooth surface, which is distinctly different from the coated ones. The matrices of both coatings display a globular and porous structure, typical of the co-sputtering technique, and are homogeneously distributed across the entire surface of the filter.

Fig. 3 shows STEM images and the corresponding EDS maps of both the coatings.

TEM images clearly reveal the morphology of the coatings, where silver nanoclusters are well visible and uniformly distributed within the silica- and zirconia-based matrices. Compared to the previous SEM observations, here the nanoclusters can be identified with higher resolution, showing very small dimensions, typically in the few-nanometer range, and a spherical shape well embedded in the matrix. In addition to these nanoclusters, some larger silver aggregates are also detected, with sizes ranging approximately from 20 to 100 nm, as confirmed by the scale markers. This morphological evidence definitively confirms the presence of metallic silver nanoclusters in both coatings, further supported by previous XRD and UV–Vis analyses that had already indicated their formation and stabilization within the matrix [33,34].

3.2. Antibacterial test

3.2.1. Inhibition halo test

The antibacterial property of the coatings was preliminarily evaluated by assessing the formation of an inhibition zone around the coated samples towards *S. epidermidis*, as shown in Fig. 4.

No inhibition halo was observed around the uncoated sample (Fig. 4a), indicating that bacteria proliferated uniformly around and in direct contact with the filter. In contrast, filters coated with SiO_2-Ag or ZrO_2-Ag coatings (Fig. 4b–c) exhibited a clearly visible zone free of bacterial colonies, demonstrating the antibacterial effect of the studied coatings. Although both matrices showed antibacterial performance, slight differences in the halo size are visible. This behaviour could be related to differences in the physicochemical properties of the oxide matrices. Silica matrices are known to provide a relatively porous structure that may facilitate the diffusion and gradual release of Ag^+ ions, while zirconia matrices generally exhibit higher chemical stability and density, as already described in Refs. [33–36]. These differences may influence the availability of silver ions at the coating surface and therefore the interaction with bacteria strain.

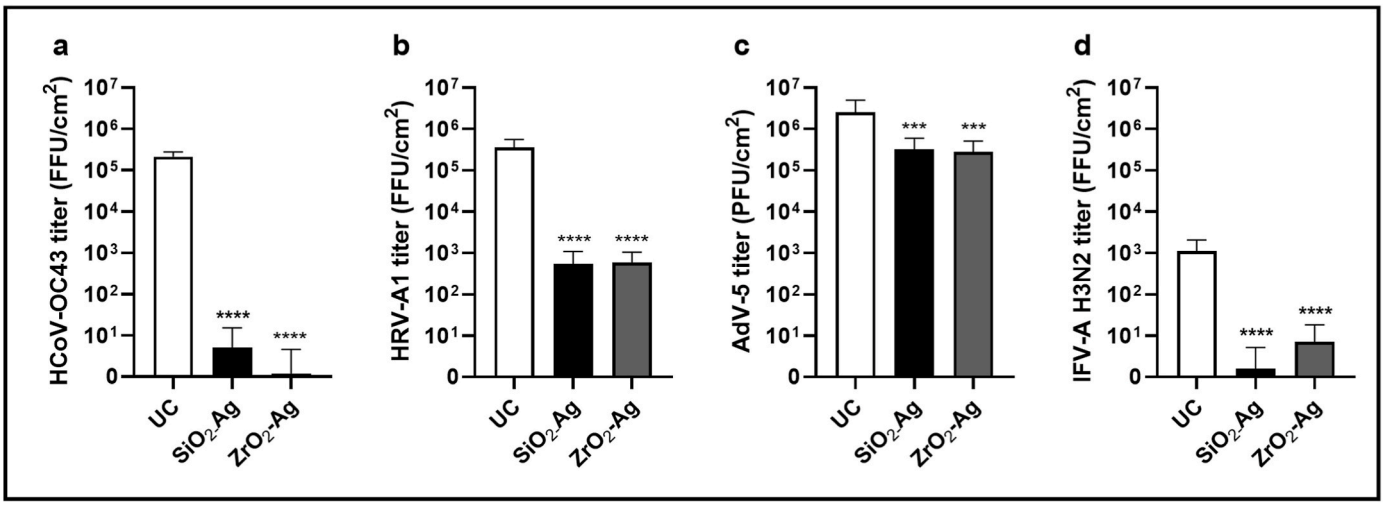

Fig. 8. *SiO_2-Ag and ZrO_2-Ag coatings exhibited a broad-spectrum antiviral activity against a panel of respiratory* viruses. Antiviral activity of SiO_2-Ag and ZrO_2-Ag coatings was tested against (a) HCoV-OC43, (b) HRV-A1, (c) AdV-5, (**d**) IFV-A H3N2. Viral titer recovered after 24h at 25 °C of virus incubation with coated or uncoated polymeric air filters is reported on the Y-axis and expressed as focus forming unit or plaque forming unit per cm^2 (FFU or PFU/cm^2). Sample type is reported on X-axis. UC, uncoated. *** pANOVA <0.001; **** pANOVA <0.0001. *The obtained results are the mean of two biological replicates*. Additional details of the assay protocol are described in the Materials and Methods section.

3.2.2. *Bacterial viability test*

The antibacterial efficacy of the filters was evaluated also by measuring the number of viable *S. aureus* bacteria after contact with the coated SiO_2-Ag and ZrO_2-Ag coated surfaces, as illustrated in Fig. 5. Bacteria were successfully recovered alive from uncoated PET filters, while significantly lower bacterial counts were obtained from SiO_2 and ZrO_2 coated filters, indicating their antibacterial activity (Table 2).

The results demonstrate that the SiO_2-Ag and ZrO_2-Ag coated filters exhibit significant antibacterial activity, exceeding 99%, as evidenced by the negligible number of viable *S. aureus* bacteria recovered from their surfaces compared to uncoated PET filters.

The antibacterial effect observed with SiO_2-Ag and ZrO_2-Ag coated filters against *S. aureus* can be attributed to the antimicrobial properties of silver (Ag) embedded in the coatings. Silver ions are known to exert a broad-spectrum antimicrobial effect by different mechanisms such as disrupting bacterial cell membranes, interfering with DNA replication, and generating reactive oxygen species that cause cellular damage [44–46]. The incorporation of SiO_2 and ZrO_2 seems to provide a stable matrix for silver, supporting the release of silver ions over time and ensuring sustained antibacterial activity. This interaction leads to the effective killing of *S. aureus* upon contact with the coated filters, preventing bacterial survival on the surface. In contrast, uncoated PET filters lack such antimicrobial properties due to the absence of silver, allowing bacteria to remain viable and to proliferate. These results are in good agreement with several studies that have previously documented the antibacterial effect of silver-containing coatings against *S. aureus* bacteria [47–49].

3.3. *Antiviral tests*

The investigation of the potential antiviral activity of SiO_2-Ag and ZrO_2-Ag coatings deposited onto polymeric air filters was conducted against a panel of four respiratory viruses: three RNA viruses, such as HCoV-OC43, IFV-A H3N2 and HRV-A1 and one DNA virus, AdV-5, following the ISO guideline.

Firstly, control tests, required by the ISO 21702:2019(E), were performed before proceeding with the evaluation of the antiviral action of the two coated materials.

The first control test complies the assessment of any cytotoxic effect of coatings on host cells, evaluating potential alterations of the treated cell monolayers. Coated filters were washed with soybean casein digest broth with lecithin and polyoxyethylene sorbitan monooleate (SCDLP broth) diluted in culture medium. In parallel experiments were performed on the uncoated substrate, as control sample.

SCDLP broth is a typical neutralizer used to inactivate antimicrobial and antiviral agents. Wash-out solutions were incubated on different cell lines at the same experimental conditions as the antiviral assays, and cellular toxicity was investigated. As shown in Fig. 6a–d, 16h incubation of pure wash-out solutions of SiO_2-Ag coating on MRC-5 (for HCoV-OC43) showed only mild toxicity, while ZrO_2-Ag coating presented no cytotoxic effect. HeLa cells were incubated with wash-out solutions for 24h (for HRV-A1) or 96h (for AdV-5). No cytotoxicity was observed on HeLa cells incubated with pure wash-out solutions of both coatings. Pure wash-out solutions incubated on MDCK for 16h (for IFV-A H3N2) did not show any toxic effect. Moreover, 1:10 diluted wash-out solutions exhibited good cytocompatibility on all cell lines.

In addition, we quantified cell viability via MTS assay, to evaluate cytotoxicity effect of coatings on cells. Viability percentages of all treated cells, per each tested condition, were reported to be >90%, confirming the promising cytocompatibility profile of both SiO_2-Ag and ZrO_2-Ag coatings (Fig. 6e–h).

According to the ISO standard, the second control test regards the verification of the cell sensitivity to virus and the inactivation of antiviral activity by SCDLP broth. Again, coated and uncoated materials were washed with diluted SCDLP broth and the control test was performed as reported in the Materials and Methods section. Next, all samples were titrated and viral titers were compared. Results are reported in Table 3 and Fig. 7.

The logarithmic difference between viral titers of wash-out solutions from SiO_2-Ag, ZrO_2-Ag, or UC, and that from NC always resulted lower than 0.5. Since the condition for the verification of the test was satisfied for all the tested viruses, the inhibitory activity of both coatings against four respiratory viruses was evaluated.

As reported in the Materials and Methods section, high-titer virus was deposited onto uncoated or coated filters and incubated for 24h at 25 °C in high-humidity conditions. After incubation, the viral titer was assessed. As additional control to determine the recovery rate (UC Imm., non-incubated virus), 400 μL of virus were deposited onto an uncoated material and immediately collected. As reported in Table 4, a slight reduction of 1 logarithm was evidenced for HCoV-OC43 and HRV-A1, recovered from the uncoated material (UC) after the incubation, compared to non-incubated virus (UC Imm).

No variation of viral titer was observed for AdV-5 with or without incubation; instead, a reduction of 2 logarithms was evidenced for IFV-A H3N2 after incubation. The variable titer of the recovered virus after 24h deposition on the uncoated material could be ascribable to two events: firstly, a weak inhibitory activity exerted by the uncoated material or a time-dependent variable persistence of viruses at 25 °C. In this context, it's well known that naked viruses, such as AdV-5 and HRV-A1, are less susceptible to environmental factors, such as desiccation, detergents, pH and temperature [50].

The strongest antiviral action was observed against HCoV-OC43: both SiO_2-Ag and ZrO_2-Ag coatings exerted a nearly complete inactivation of HCoV-OC43 with an R value of 4.26 for SiO_2-Ag (inhibition %: 99.99) and 5.26 for ZrO_2-Ag (inhibition %: 99.99). Similarly, both coatings displayed an almost total inhibition of IFV-A H3N2 with an R value of 2.88 for SiO_2-Ag (inhibition %: 99.87) and 2.22 for ZrO2-Ag (inhibition %: 99.40). A statistically significant antiviral activity of both coatings was evidenced also against HRV-A1 with an R value of 2.81 for SiO_2-Ag (inhibition %: 99.84) and 2.79 for ZrO_2-Ag (inhibition %: 99.84). Lastly, a partial, albeit significant, inhibition of AdV-5 infectivity was observed with an R value of 0.94 for SiO_2-Ag (inhibition %: 88.48) and 0.79 for ZrO_2-Ag (inhibition %: 83.68). Overall, these data demonstrated that both SiO_2-Ag and ZrO_2-Ag coatings deposited onto polymeric air filters are endowed with broad-spectrum antiviral action against four respiratory viruses that belong to different viral families: HCoV-OC43 to the *Coronaviridae* family, HRV-A1 to the *Picornaviridae* family, AdV-5 to the *Adenoviridae* family and IFV-A H3N2 to the *Orthomyxoviridae* family. In detail, the two coatings exerted a comparable inhibitory activity with similar R values and inhibition percentages per each tested virus (Table 4).

A summary of the antiviral activity of SiO_2-Ag and ZrO_2-Ag against the four tested respiratory viruses is reported in Table 5. Notably, coatings were able to reduce the infection of both enveloped viruses (HCoV-OC43 and IFV-A H3N2) and naked viruses (HRV-A1 and AdV-5). This last activity is particularly relevant, given the known high resistance of non-enveloped viruses to environmental conditions and thereby it highlights the potentiality of the present coatings.

Fig. 8 reported the antiviral activity exerted by coated samples compared to the uncoated ones after incubation.

The reliability of our data is confirmed by previous studies that demonstrated the potential antibacterial and antiviral activity of silver nanoclusters/silica composite coating deposited onto multiple materials, such as glass fiber, metallic, or polymeric ones and cotton textiles [34,36]. In particular, *Luceri* et al. demonstrated that the anti-coronavirus action of SiO_2-Ag coating was partially due to its virucidal effect and to the release of silver ions from the coating [34]. The relevance of this work lies in the systematic assessment and demonstration of antiviral activity of Ag-nanocluster composite coatings applied to air filtration media, evaluated against both enveloped and non-enveloped viruses, following the ISO 21702:2019(E) guideline protocols, together with a favourable cytocompatibility profile on tested cells.

Additionally, these results are particularly relevant in light of their potential practical application. Specifically, the use of antibacterial and antiviral coatings in air filtration systems offers a promising and scalable approach to reduce the airborne transmission of respiratory viruses from different families in crowded indoor settings.

Due to these interesting ad promising results, further studies are ongoing to clarify the mechanism of action of SiO_2-Ag and ZrO_2-Ag coatings. In particular, shorter incubation times will be tested to determine whether the antiviral activity is maintained even with a brief contact of the virus onto the material. Moreover, assays will be carried out to discriminate if the observed antiviral action is mediated by an indirect activity due to ions potentially released from the coatings, or rather by a direct mechanism involving morphological damage or physical trapping of the viral particle upon contact with the coated surfaces.

4. Conclusions

In the present work, composite coatings in silica or zirconia matrix, embedding silver nanoclusters, SiO_2-Ag and ZrO_2-Ag coatings, were developed and deposited through the PVD co-sputtering method on PET materials, intended for air filtration systems. Morphological and compositional analysis revealed the formation of silver nanoclusters homogeneously distributed in the two matrices. Antibacterial tests demonstrate the antibacterial effectiveness of silver-based coatings on silica (SiO_2-Ag) and zirconia (ZrO_2-Ag) matrices against *S. epidermidis* and *S. aureus*. Unlike the uncoated PET filters, which allowed bacterial proliferation, the coated filters exhibited strong bactericidal activity, achieving over 99% reduction in bacterial viability, as confirmed by both viability assays and the presence of inhibition halos. These findings highlight the potential of such coatings for applications requiring effective antimicrobial surfaces. Antiviral tests demonstrate that both SiO_2-Ag and ZrO_2-Ag coatings exhibited an effect against a broad-spectrum of viruses, both enveloped and naked. The strongest effect was achieved by both coatings against HCoV-OC43, (inhibition %: 99.99); an almost total inhibition was exhibited against of IFV-A H3N2 and HRV-A1; AdV-5 infectivity was partially inhibited, reaching anyway significant results.

CRediT authorship contribution statement

Domiziana Porporato: Writing – review & editing, Writing – original draft, Validation, Investigation. **Angelica Luceri:** Writing – review & editing, Writing – original draft, Validation, Investigation. **Elisa Feyles:** Writing – review & editing, Validation, Investigation. **David Lembo:** Writing – review & editing, Visualization, Supervision, Funding acquisition. **Manuela Donalisio:** Writing – review & editing, Visualization, Supervision, Conceptualization. **Borja Coto:** Writing – review & editing, Supervision, Investigation. **Sofia Alves:** Writing – review & editing, Validation, Investigation. **Olatz Areitioaurtena:** Writing – original draft, Validation, Investigation. **Per Persson:** Investigation. **Cristina Balagna:** Writing – review & editing, Visualization, Supervision, Funding acquisition, Conceptualization.

Declaration of competing interest

The authors declare that they have no known competing financial interests or personal relationships that could have appeared to influence the work reported in this paper.

Acknowledgement

This work has received funding from the European Commission Horizon Europe programme under grant agreement n. 101057597 (NANOBLOC - Antiviral, antibacterial & antifungal nanocoating platform)

References

[1] K.-H. Kim, E. Kabir, S.A. Jahan, Airborne bioaerosols and their impact on human health, J. Environ. Sci. China 67 (2018) 23–35, https://doi.org/10.1016/j.jes.2017.08.027.

[2] S. Su, G. Wong, W. Shi, J. Liu, A.C.K. Lai, J. Zhou, W. Liu, Y. Bi, G.F. Gao, Epidemiology, genetic recombination, and pathogenesis of coronaviruses, Trends Microbiol. 24 (6) (2016) 490–502, https://doi.org/10.1016/j.tim.2016.03.003.

[3] C. Esneau, A.C. Duff, N.W. Bartlett, Understanding Rhinovirus circulation and impact on illness, Viruses 14 (1) (2022) 141, https://doi.org/10.3390/v14010141.

[4] R. Hewitt, H. Farne, A. Ritchie, E. Luke, S.L. Johnston, P. Mallia, The role of viral infections in exacerbations of chronic obstructive pulmonary disease and asthma, Ther. Adv. Respir. Dis. 10 (2) (2016) 158–174, https://doi.org/10.1177/1753465815618113.

[5] Influenza (seasonal). https://www.who.int/news-room/fact-sheets/detail/influenza-(seasonal. (Accessed 25 March 2025).

[6] B.J. Jester, T.M. Uyeki, D.B. Jernigan, Fifty years of Influenza A(H3N2) following the pandemic of 1968, Am. J. Public Health 110 (5) (2020) 669–676, https://doi.org/10.2105/AJPH.2019.305557.

[7] M. Hatherill, M. Levin, J. Lawrenson, N.-Y. Hsiao, L. Reynolds, A. Argent, Evolution of an adenovirus outbreak in a multidisciplinary children's hospital, J. Paediatr. Child Health 40 (8) (2004) 449–454, https://doi.org/10.1111/j.1440-1754.2004.00426.x.

[8] C.C. Wang, K.A. Prather, J. Sznitman, J.L. Jimenez, S.S. Lakdawala, Z. Tufekci, L. C. Marr, Airborne transmission of respiratory viruses, Science 373 (6558) (2021), https://doi.org/10.1126/science.abd9149 eabd9149.

[9] J.S. Kutter, M.I. Spronken, P.L. Fraaij, R.A. Fouchier, S. Herfst, Transmission routes of respiratory viruses among humans, Curr. Opin. Virol. 28 (2018) 142–151, https://doi.org/10.1016/j.coviro.2018.01.001.

[10] D.K. Milton, M.P. Fabian, B.J. Cowling, M.L. Grantham, J.J. McDevitt, Influenza virus aerosols in human exhaled breath: particle size, culturability, and effect of surgical masks, PLoS Pathog. 9 (3) (2013) e1003205, https://doi.org/10.1371/journal.ppat.1003205.

[11] L. Guoliang, M. Xiao, X. Zhang, C. Gal, X. Chen, L. Liu, S. Pan, J. Wu, L. Tang, D. Clements-Croome, A review of air filtration technologies for sustainable and healthy building ventilation, Sustain. Cities Soc. 32 (2017), https://doi.org/10.1016/j.scs.2017.04.011.

[12] A.A.I.A.S. Komaladewi, K. Khoiruddin, I.W. Surata, I.D.G.A. Subagia, I.G. Wenten, Recent advances in antimicrobial air filter, in: E3S Web Conf., vol. 67, 2018 03016, https://doi.org/10.1051/e3sconf/20186703016.

[13] J. Guo, Y. Xiong, T. Kang, Z. Xiang, C. Qin, Bacterial community analysis of floor dust and HEPA filters in air purifiers used in office rooms in ILAS, Beijing, Sci. Rep. 10 (1) (2020) 6417, https://doi.org/10.1038/s41598-020-63543-1.

[14] S.K. Park, S.Y. Lee, S.B. Kim, I.H. Kim, D.U. Lee, J.H. Shin, J.S. Son, G. Kim, S. H. Yoo, D.Y. Lee, J.H. Jung, D.Y. Choi, Dual-action antibacterial nanoblades for rapid inactivation of bioaerosols in personal protective equipment, Adv. Funct. Mater. 35 (30) (2025) 2421728, https://doi.org/10.1002/adfm.202421728.

[15] S.Y. Lee, J.H. Shin, I.H. Kim, D.Y. Choi, D.U. Lee, G.B. Hwang, B. Han, S.B. Kim, D.-K. Song, I. Park, J.H. Jung, Transparent and visible light-activated antimicrobial air filters from electrospun crystal violet-embedded polyacrylonitrile nanofibers, Environ. Res. 266 (2025) 120490, https://doi.org/10.1016/j.envres.2024.120490.

[16] S.B. Jeong, K.J. Heo, J.H. Yoo, D.-G. Kang, L. Santoni, C.E. Knapp, A. Kafizas, C. J. Carmalt, I.P. Parkin, J.H. Shin, G.B. Hwang, J.H. Jung, Photobiocidal activity of TiO_2/UHMWPE composite activated by reduced graphene oxide under white light, Nano Lett. 24 (30) (2024) 9155–9162, https://doi.org/10.1021/acs.nanolett.4c00939.

[17] S.B. Jeong, D.U. Lee, B.J. Lee, K.J. Heo, D.W. Kim, G.B. Hwang, A.J. MacRobert, J. H. Shin, H.S. Ko, S.K. Park, Y.S. Oh, S.J. Kim, D.Y. Lee, S.-B. Lee, I. Park, S.B. Kim, B. Han, J.H. Jung, D.Y. Choi, Photobiocidal-Triboelectric nanolayer coating of Photosensitizer/Silica-alumina for reusable and visible-light-driven Antibacterial/Antiviral air filters, Chem. Eng. J. 440 (2022) 135830, https://doi.org/10.1016/j.cej.2022.135830.

[18] D.U. Lee, S.B. Jeong, B.J. Lee, S.K. Park, H.-M. Kim, J.H. Shin, S.Y. Lee, G. Kim, J. Park, G.M. Kim, J.H. Jung, D.Y. Choi, Antimicrobial and antifouling effects of petal-like nanostructure by evaporation-induced self-assembly for personal protective equipment, Small 20 (14) (2024) 2306324.

[19] B. Song, E. Zhang, X. Han, H. Zhu, Y. Shi, Z. Cao, Engineering and application perspectives on designing an antimicrobial surface, ACS Appl. Mater. Interfaces 12 (19) (2020) 21330–21341, https://doi.org/10.1021/acsami.9b19992.

[20] A. Luceri, R. Francese, D. Lembo, M. Ferraris, C. Balagna, Silver nanoparticles: review of antiviral properties, mechanism of action and applications, Microorganisms 11 (3) (2023) 629, https://doi.org/10.3390/microorganisms11030629.

[21] X.-F. Zhang, Z.-G. Liu, W. Shen, S. Gurunathan, Silver nanoparticles: synthesis, characterization, properties, applications, and therapeutic approaches, Int. J. Mol. Sci. 17 (9) (2016) 1534, https://doi.org/10.3390/ijms17091534.

[22] Z.A. Ratan, F.R. Mashrur, A.P. Chhoan, S. Md Shahriar, M.F. Haidere, N.J. Runa, S. Kim, D.-H. Kweon, H. Hosseinzadeh, J.Y. Cho, Silver nanoparticles as potential antiviral agents, Pharmaceutics 13 (12) (2021) 2034, https://doi.org/10.3390/pharmaceutics13122034.

[23] F. Pilaquinga, J. Morey, M. Torres, R. Seqqat, M.D.L.N. Piña, Silver nanoparticles as a potential treatment against SARS-CoV -2: a review, WIREs Nanomedicine Nanobiotechnol. 13 (5) (2021) e1707, https://doi.org/10.1002/wnan.1707.

[24] D.H. Park, J. Hwang, D. Shin, Y. Kim, G. Lee, I. Park, S.B. Kim, K. Hong, B. Han, Developing an optimal antiviral method for the air-filtration system of subway stations, Aerosol Air Qual. Res. 23 (8) (2023) 230088, https://doi.org/10.4209/aaqr.230088.

[25] D.H. Park, Y.H. Joe, J. Hwang, Dry aerosol coating of anti-viral particles on commercial air filters using a high-volume flow atomizer, Aerosol Air Qual. Res. 19 (7) (2019) 1636–1644, https://doi.org/10.4209/aaqr.2019.04.0212.

[26] H.R. Byun, S.Y. Park, E.T. Hwang, B.I. Sang, J. Min, D. Sung, W.I. Choi, S. Kim, J. H. Lee, Antimicrobial air filter coating with plant extracts against airborne microbes, Appl. Sci. 10 (24) (2020) 9120, https://doi.org/10.3390/app10249120.

[27] D. Druvari, I. Tzoumani, Z. Piperigkou, K. Tzaferi, D. Tselentis, A. Vlamis-Gardikas, N.K. Karamanos, G. Bokias, J.K. Kallitsis, Development of environmentally friendly biocidal coatings based on water-soluble copolymers for air-cleaning filters, ACS Omega 7 (39) (2022) 35204–35216, https://doi.org/10.1021/acsomega.2c04427.

[28] H. Ghazal, N. Sohail, H. Ghazal, N. Sohail, Sputtering deposition, in: Thin Films - Deposition Methods and Applications, IntechOpen, 2022, https://doi.org/10.5772/intechopen.107353.

[29] A. Baptista, F.J.G. Silva, J. Porteiro, J.L. Míguez, G. Pinto, L. Fernandes, On the physical vapour deposition (PVD): evolution of magnetron sputtering processes for industrial applications, Procedia Manuf. 17 (2018) 746–757, https://doi.org/10.1016/j.promfg.2018.10.125.

[30] G.E. Stan, M. Montazerian, A. Shearer, B.W. Stuart, F. Baino, J.C. Mauro, J.M. F. Ferreira, Critical advances in the field of magnetron sputtered bioactive glass thin-films: an analytical review, Appl. Surf. Sci. 646 (2024) 158760, https://doi.org/10.1016/j.apsusc.2023.158760.

[31] L. Reyes-Carmona, O.A. Sepúlveda-Robles, A. Almaguer-Flores, J.M. Bello-Lopez, C. Ramos-Vilchis, S.E. Rodil, Antimicrobial activity of silver-copper coating against aerosols containing surrogate respiratory viruses and bacteria, PLoS One 18 (12) (2023) e0294972, https://doi.org/10.1371/journal.pone.0294972.

[32] X. Huang, Q. Hu, J. Li, W. Yao, C. Wang, Y. Feng, W. Song, Sputtering-deposited ultra-thin Ag–Cu films on non-woven fabrics for face masks with antimicrobial function and breath NOx response, Materials 17 (7) (2024) 1574, https://doi.org/10.3390/ma17071574.

[33] A. Luceri, S. Perero, A. Cochis, A.C. Scalia, L. Rimondini, M. Ferraris, C. Balagna, Washing resistant antibacterial composite coatings on cotton textiles, Cellulose 30 (15) (2023) 9877–9897, https://doi.org/10.1007/s10570-023-05471-7.

[34] A. Luceri, R. Francese, S. Perero, D. Lembo, M. Ferraris, C. Balagna, Antibacterial and antiviral activities of silver Nanocluster/Silica composite coatings deposited onto air filters, ACS Appl. Mater. Interfaces 16 (3) (2024) 3955–3965, https://doi.org/10.1021/acsami.3c13843.

[35] C. Balagna, S. Perero, F. Bosco, C. Mollea, M. Irfan, M. Ferraris, Antipathogen nanostructured coating for air filters, Appl. Surf. Sci. 508 (2020) 145283, https://doi.org/10.1016/j.apsusc.2020.145283.

[36] C. Balagna, R. Francese, S. Perero, D. Lembo, M. Ferraris, Nanostructured composite coating endowed with antiviral activity against human respiratory viruses deposited on fibre-based air filters, Surf. Coat. Technol. 409 (2021) 126873, https://doi.org/10.1016/j.surfcoat.2021.126873.

[37] M. Ferraris, C. Balagna, S. Perero, Method for the application of an antiviral coating to a substrate and relative coating, WO2019082001A1.

[38] A. Verbič, M. Gorjanc, B. Simončič, Zinc oxide for functional textile coatings: recent advances, Coatings 9 (9) (2019) 550, https://doi.org/10.3390/coatings9090550.

[39] ISO 20743, Textiles-Determination of Antibacterial Activity of Textile Produts, 2022.

[40] ISO 22196, Measurement of Antibacterial Activity on Plastic and Other Non-porous Surfaces, 2011.

[41] S. Baroni, T. Carletti, M. Donalisio, I. Arduino, I. Cazzaniga, T. Giorgino, F. Esposito, A. Porta, L. Diomede, A. De Luigi, M. Gobbi, D. Lembo, A. Marcello, E. Tramontano, M. Milani, E. Mastrangelo, The antipsychotic drug lurasidone inhibits coronaviruses by affecting multiple targets, Front. Cell. Infect. Microbiol. 14 (2024) 1487604, https://doi.org/10.3389/fcimb.2024.1487604.

[42] ISO 21702:2019(en), Measurement of Antiviral Activity on Plastics and Other Non-porous Surfaces.

[43] R. Francese, A. Civra, M. Rittà, M. Donalisio, M. Argenziano, R. Cavalli, A. S. Mougharbel, U. Kortz, D. Lembo, Anti-Zika virus activity of polyoxometalates, Antivir. Res. 163 (2019) 29–33, https://doi.org/10.1016/j.antiviral.2019.01.005.

[44] Q.L. Feng, J. Wu, G.Q. Chen, F.Z. Cui, T.N. Kim, J.O. Kim, A mechanistic study of the antibacterial effect of silver ions on Escherichia Coli and Staphylococcus Aureus, J. Biomed. Mater. Res. 52 (4) (2000) 662–668, https://doi.org/10.1002/1097-4636(20001215)52:4%253C662::aid-jbm10%253E3.0.co;2-3.

[45] W.K. Jung, H.C. Koo, K.W. Kim, S. Shin, S.H. Kim, Y.H. Park, Antibacterial activity and mechanism of action of the silver ion in *Staphylococcus Aureus* and *Escherichia Coli*, Appl. Environ. Microbiol. 74 (7) (2008) 2171–2178, https://doi.org/10.1128/AEM.02001-07.

[46] M.A. Quinteros, C.A. Viviana, R. Onnainty, V.S. Mary, M.G. Theumer, G. E. Granero, M.G. Paraje, P.L. Páez, Biosynthesized silver nanoparticles: decoding their mechanism of action in Staphylococcus Aureus and Escherichia Coli, Int. J. Biochem. Cell Biol. 104 (2018) 87–93, https://doi.org/10.1016/j.biocel.2018.09.006.

[47] F.J. Geissel, V. Platania, A. Gogos, I.K. Herrmann, G.N. Belibasakis, M. Chatzinikolaidou, G.A. Sotiriou, Antibiofilm activity of nanosilver coatings against *Staphylococcus Aureus*, J. Colloid Interface Sci. 608 (2022) 3141–3150, https://doi.org/10.1016/j.jcis.2021.11.038.

[48] S. Kii, H. Miyamoto, M. Ueno, I. Noda, A. Hashimoto, T. Nakashima, T. Shobuike, S. Kawano, M. Sonohata, M. Mawatari, Long-term antibacterial activity of silver-containing hydroxyapatite coatings against *Staphylococcus aureus in vitro* and *in Vivo*, J. Orthop. Sci. 29 (6) (2024) 1503–1512, https://doi.org/10.1016/j.jos.2023.10.009.

[49] J. Osés, J.F. Palacio, S. Kulkarni, A. Medrano, J.A. García, R. Rodríguez, Antibacterial PVD coatings doped with silver by ion implantation, Appl. Surf. Sci. 310 (2014) 56–61, https://doi.org/10.1016/j.apsusc.2014.04.043.

[50] J.E. Wißmann, L. Kirchhoff, Y. Brüggemann, D. Todt, J. Steinmann, E. Steinmann, Persistence of pathogens on inanimate surfaces: a narrative review, Microorganisms 9 (2) (2021) 343, https://doi.org/10.3390/microorganisms9020343.